Article

Not peer-reviewed version

Ultrastructural Characterization of Lipid-Rich and Vesicle-Like Structures in *Leishmania* (*L.*) *amazonensis*

Áurea Martins Gabriel *, Adan Galué-Parra, Washington Luiz Assunção Pereira, Ketil Winther Pedersen, Edilene Oliveira da Silva

Posted Date: 25 February 2026

doi: 10.20944/preprints202602.1539.v1

Keywords: *Leishmania amazonensis*; lipid-rich structures; vesicle-like compartments; ultrastructure; TEM; SEM; BODIPY; NTA

Article

Ultrastructural Characterization of Lipid-Rich and Vesicle-Like Structures in *Leishmania* (*L.*) *amazonensis*

Áurea Martins Gabriel [1,2,*], Adan Galué-Parra [2], Washington Luiz Assunção Pereira [3], Ketil Winther Pedersen [4] and Edilene Oliveira da Silva [2,5]

[1] Global Health and Tropical Medicine (GHTM), Institute of Hygiene and Tropical Medicine, NOVA University of Lisbon (IHMT-UNL), 1349-008 Lisbon, Portugal

[2] Institute of Biological Sciences, Federal University of Pará (UFPA), Av. Augusto Correa 01, 66075-110 Belém, PA, Brazil

[3] Laboratory of Animal Pathology, Federal Rural University of Amazon (UFRA), 66077-830 Belém, PA, Brazil

[4] Thermo Fisher Scientific, 0379 Oslo, Norway

[5] National Center for Structural Biology and Bioimaging (CENABIO), 21941-902 Rio de Janeiro, RJ, Brazil

* Correspondence: aurealinharesm@gmail.com

Abstract

Lipid-rich structures are frequently observed in *Leishmania* spp., yet their morphological diversity and stage-specific distribution remain insufficiently described. Here, we performed an ultrastructural and fluorescence-based characterization of *Leishmania* (*L.*) *amazonensis* promastigotes and intracellular amastigotes using transmission electron microscopy (TEM), scanning electron microscopy (SEM), BODIPY® lipid staining, and Nanoparticle Tracking Analysis (NTA). Promastigotes exhibited vesicle-like and membrane-derived compartments concentrated in the flagellar pocket, as well as electron-dense lipid bodies adjacent to the Golgi complex. Intracellular amastigotes displayed rounded morphology within parasitophorous vacuoles and contained distinct lipid-rich inclusions. BODIPY staining confirmed neutral lipid pools in promastigotes. NTA detected submicron particles in culture supernatants, with amastigotes showing higher particle abundance (3.1–5.9 × 10^8 particles/mL) and smaller mean sizes (132–171 nm) compared with promastigotes. These observations provide a descriptive account of lipid-rich and vesicle-like structures in *L. amazonensis* and offer morphological context for future investigations into membrane dynamics, lipid metabolism, and parasite–host interactions. No inference of vesicle identity, biogenesis, or function is made, in accordance with MISEV2023 recommendations.

Keywords: *Leishmania amazonensis*; lipid-rich structures; vesicle-like compartments; ultrastructure; TEM; SEM; BODIPY; NTA

1. Introduction

Leishmania spp. are intracellular protozoan parasites responsible for a spectrum of neglected tropical diseases with substantial global impact [1–3]. Their ability to survive and proliferate within macrophages reflects a suite of evolutionary adaptations involving membrane remodelling, metabolic flexibility, and stage-specific structural organization [4–8]. Lipids play central roles in these processes, contributing to membrane architecture, organelle dynamics, vesicle formation, and stress responses [4,9,10]. Despite their importance, the morphological distribution of lipid-rich structures in *Leishmania* remains insufficiently documented, particularly in *L. (L.) amazonensis*, a species associated with diffuse cutaneous leishmaniasis and characterized by large parasitophorous vacuoles and attenuated macrophage microbicidal activity [11,12].

 doi:10.20944/preprints202602.1539.v1

Previous studies have described lipid bodies, membrane-derived compartments, and autophagy-related structures in trypanosomatids, suggesting that lipid reservoirs may support membrane turnover, metabolic adaptation, or responses to environmental stress [13–16]. In parallel, extracellular vesicles released by *Leishmania* (*L*EVs) have emerged as key mediators of parasite–host communication, transporting proteins, lipids, and nucleic acids capable of modulating immune signalling and promoting infection [1,2,9,10,17–20]. Although the protein and RNA cargo of *L*EVs has been extensively characterized, their lipid composition and the structural diversity of intracellular lipid-rich compartments remain comparatively underexplored [21–24].

Morphological approaches such as transmission electron microscopy (TEM), scanning electron microscopy (SEM), and fluorescence microscopy provide essential tools for documenting the spatial organization of lipid-rich and vesicle-like structures across parasite stages [12,13]. Complementary biophysical methods, including Nanoparticle Tracking Analysis (NTA), enable the quantification of submicron particles present in culture supernatants without inferring their identity or origin, in alignment with current MISEV2023 recommendations for descriptive particle analysis [23].

In this study, we performed an ultrastructural and fluorescence-based characterization of promastigotes and intracellular amastigotes of *L. (L.) amazonensis*. We additionally applied NTA to describe the size distribution and abundance of particles present in the extracellular environment of each stage. Our aim was not to define vesicle biogenesis or function, but rather to provide a descriptive account of lipid-rich and vesicle-like structures that may inform future mechanistic studies on membrane dynamics and parasite–host interactions.

Finally, lipid-mediated communication between parasite and host can be contextualized within a One Health framework, which recognizes that parasitic diseases emerge and persist through interconnected human, animal, and environmental systems [11]. This conceptual relationship is illustrated in Figure 1 as a schematic framework rather than a direct experimental outcome.

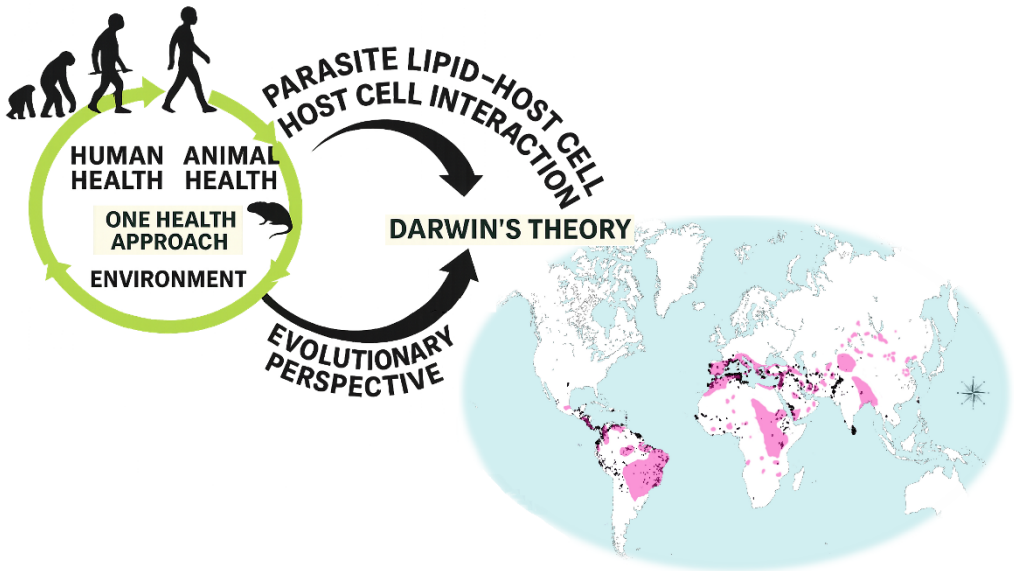

Figure 1. Conceptual diagram illustrates evolutionary principles relevant to Leishmania research. The central theme of natural selection is represented by hominid silhouettes, with arrows indicating five theoretical domains: EvoDevo, Neodarwinism, Niche Theory, Epigenetics, and RQT Red Queen coevolutionary dynamics. A world map depicts the global distribution of zoonotic Leishmania species. This figure provides a conceptual framework and does not represent experimental data—and complements the comparative information presented in Supplementary Table S1.

 doi:10.20944/preprints202602.1539.v1

2. Materials and Methods

2.1. Parasite Culture

Leishmania (*L.*) *amazonensis* (MHOM/BR/26361) promastigotes were maintained in RPMI 1640 medium supplemented with 10% fetal bovine serum (FBS) at 27 °C in a Biological Oxygen Demand (B.O.D.) incubator. Cultures were monitored daily, and exponential-phase (day 4) and stationary-phase (day 7) promastigotes were collected according to the experimental design. Parasites were centrifuged at 2,500 rpm for 10 min at 27 °C, resuspended in fresh medium, and quantified using a Neubauer chamber. All experiments were performed using a single strain to ensure methodological consistency across parasite stages.

2.2. Animals and Peritoneal Macrophage Isolation

Male BALB/c mice (6–8 weeks old) were euthanized in a CO_2 chamber following CONCEA guidelines. Peritoneal macrophages were harvested by lavage with 5 mL of sterile DMEM, centrifuged at 1,500 rpm for 10 min, and resuspended in serum-free DMEM. Cells were seeded onto sterile glass coverslips and incubated at 37 °C with 5% CO_2 for 2 h to allow adhesion. Non-adherent cells were removed by PBS washing, and adherent macrophages were maintained in DMEM supplemented with 10% FBS for 24 h before infection.

2.3. Macrophage Infection

Stationary-phase promastigotes were added to macrophage monolayers at a 10:1 parasite-to-cell ratio. After 4 h of interaction, non-internalized parasites were removed by PBS washing. Infected cultures were incubated for 24–48 h at 37 °C with 5% CO_2.

2.4. Light Microscopy and Giemsa Staining

2.4.1. Promastigotes

Promastigotes (1×10^6 cells/mL) were fixed with 3% paraformaldehyde (PFA) and adhered to poly-L-lysine–coated coverslips for 30 min. Samples were stained with 10% Giemsa (pH 8.0) for 30 min and imaged using an Olympus BX41 microscope equipped with a Zeiss digital camera.

2.4.2. Intracellular Amastigotes

Infected macrophages were fixed with either 3% PFA in 0.1 M PHEM buffer or cold methanol. Samples were stained with Giemsa for 30 min, rinsed, air-dried, and mounted. Images were acquired using an Olympus BX41 microscope.

2.5. Scanning Electron Microscopy (SEM)

Macrophages (10^6 cells/mL) infected for 72 h were fixed with 2.5% glutaraldehyde, dehydrated in graded ethanol, and critical-point dried. The upper macrophage surface was gently removed with adhesive tape to expose parasitophorous vacuoles. Samples were sputter-coated with gold and examined using a MIRA 3 TESCAN SEM.

2.6. Transmission Electron Microscopy (TEM)

Promastigotes (2×10^6 cells/mL) were fixed in 2.5% glutaraldehyde, 4% PFA, and 2.5% sucrose in 0.1 M cacodylate buffer (pH 7.2). Post-fixation was performed with 1% osmium tetroxide and 0.8% potassium ferrocyanide. Samples were dehydrated in acetone, embedded in Epon®, sectioned using a Leica EM UC6 ultramicrotome, stained with uranyl acetate and lead citrate, and examined using a LEO 906 E TEM.

 doi:10.20944/preprints202602.1539.v1

2.7. Bodipy Lipid Staining

Fixed promastigotes were permeabilized with 1% Triton X-100, blocked with 50 mM NH_4Cl, and stained with BODIPY® 493/503 (1 µg/mL) for 15 min in the dark. Nuclei were counterstained with DAPI. Fluorescence images were acquired using FITC and DAPI filters on a Zeiss Axio Scope.A1 microscope.

2.8. Nanoparticle Tracking Analysis (NTA)

Culture supernatants from promastigotes (days 4 and 7) and infected macrophages (24–48 h) were collected, centrifuged to remove debris, and filtered through 0.22 µm membranes. All samples were processed using exosome-depleted (ExoFree) medium following standardized IHMT protocols. Additional workflows included Total Exosome Isolation kits and a combined filtration–ultrafiltration–ExoSpin protocol.

Samples were diluted to 1×10^8–1×10^9 particles/mL and analyzed using a NanoSight instrument (488 nm laser). Three 60 s videos were recorded per sample at 25 °C under identical settings. Particle concentration and size distribution were calculated using automated tracking software. All measurements were performed in technical triplicates and reported descriptively, without inference of vesicle identity, in accordance with MISEV2023.

3. Results

3.1. Promastigote Morphology

Stationary-phase promastigotes displayed elongated bodies with externalized flagella (Figure 2A). TEM revealed abundant vesicle-like structures concentrated in the flagellar pocket, along with electron-dense lipid-rich inclusions adjacent to the Golgi complex (Figure 4A).

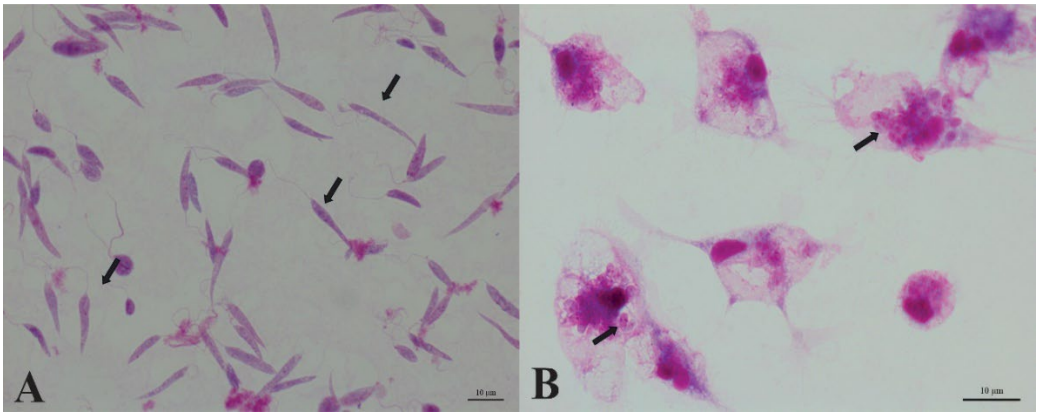

Figure 2. Light microscopy of Leishmania (L.) amazonensis. (A) Stationary-phase promastigotes showing elongated bodies and externalized flagella (arrows). (B) Mouse peritoneal macrophages containing intracellular amastigotes within parasitophorous vacuoles (arrows). Samples were stained with Giemsa.

3.2. Intracellular Amastigotes

Giemsa staining confirmed intracellular amastigotes within parasitophorous vacuoles (Figure 2B). SEM imaging revealed rounded amastigotes with surface protrusions, consistent with intracellular adaptation (Figure 3).

3.3. Lipid-Rich Structures

Both parasite stages exhibited electron-dense lipid bodies located near the flagellar pocket and Golgi region (Figure 4). Promastigotes also displayed Golgi-associated cisternal structures compatible with early autophagic processes (Figure 5).

 doi:10.20944/preprints202602.1539.v1

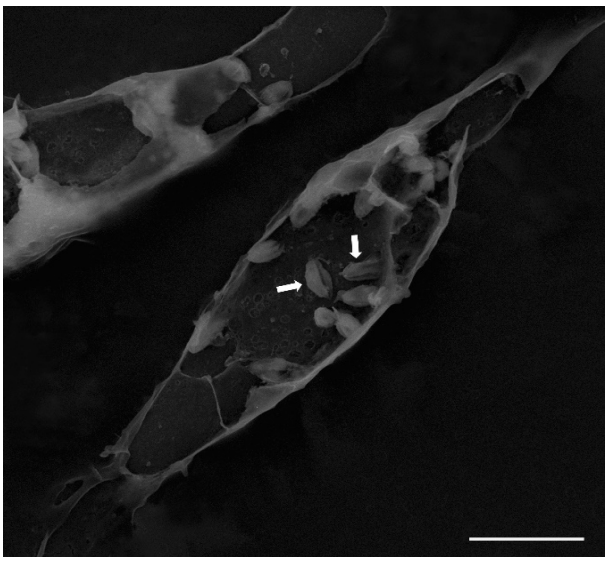

Figure 3. Scanning electron microscopy (SEM) of infected macrophages. SEM micrograph showing intracellular amastigotes (arrows) within parasitophorous vacuoles after 72 h of infection.

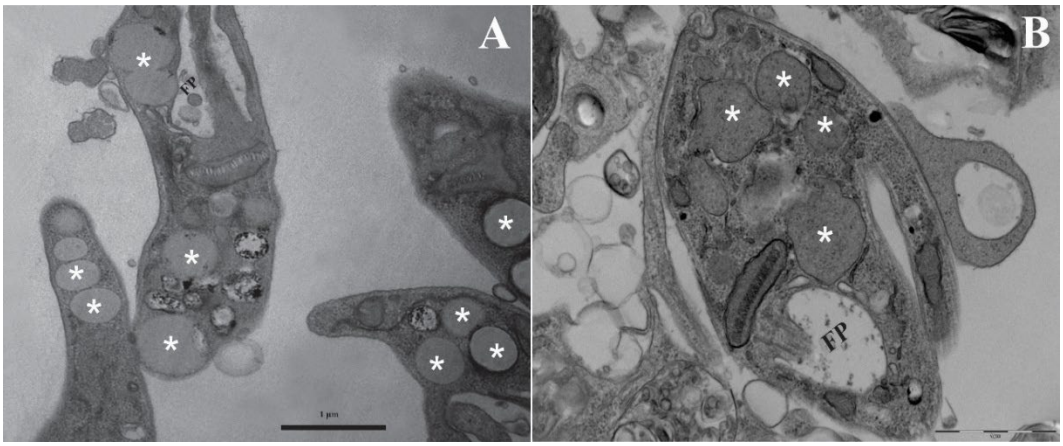

Figure 4. Ultrastructural features of lipid-rich structures in *Leishmania* (*L.*) *amazonensis.* (A) Promastigote showing electron-dense lipid bodies (*) *near the flagellar pocket (FP).* B) Intracellular amastigote displaying lipid-rich inclusions (*) TEM.

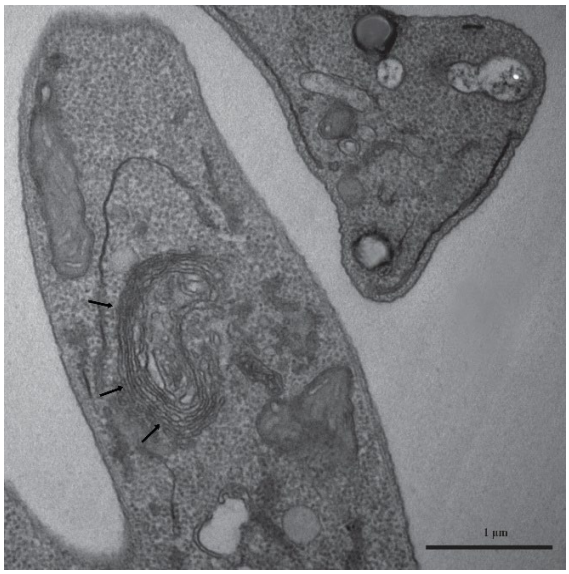

 doi:10.20944/preprints202602.1539.v1

Figure 5. Golgi-associated cisternal structures in promastigotes. TEM micrograph showing Golgi cisternae with features compatible with early autophagic processes.

3.4. Bodipy Staining

Fluorescence microscopy confirmed the presence of neutral lipid bodies in promastigotes, with BODIPY® 493/503 labeling producing punctate cytoplasmic signals (Figure 6).

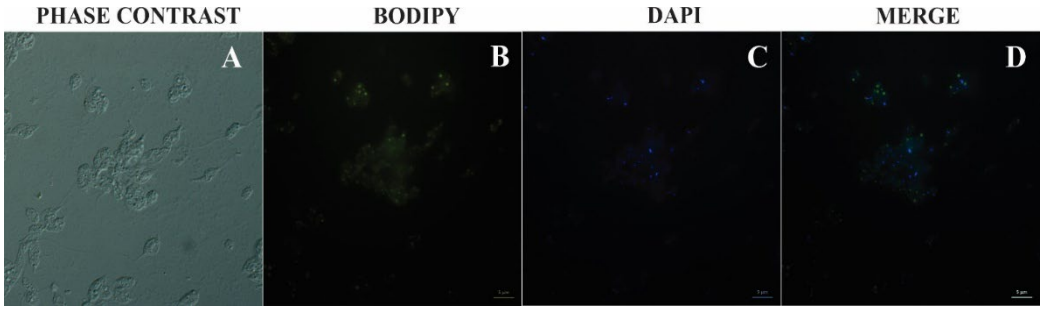

Figure 6. BODIPY® 493/503 staining of neutral lipid bodies in promastigotes. (A) Phase-contrast image. (B) BODIPY-labeled lipid bodies. (C) DAPI-stained nuclei. (D) Merged image showing colocalization of nuclear and lipid signals.

3.5. Nanoparticle Tracking Analysis (NTA)

NTA detected submicron particles in all supernatants. Amastigote-derived samples exhibited higher concentrations (3.1–5.9 × 10^8 particles/mL) and smaller mean sizes (132–171 nm), whereas promastigote samples showed broader distributions and larger modal diameters (~241 nm). The filtration–ultrafiltration–ExoSpin workflow revealed two predominant peaks (~60–70 nm and ~150–160 nm) in both stages (Figure 7). All measurements remained within analytical limits and were interpreted descriptively, without assigning vesicle identity.

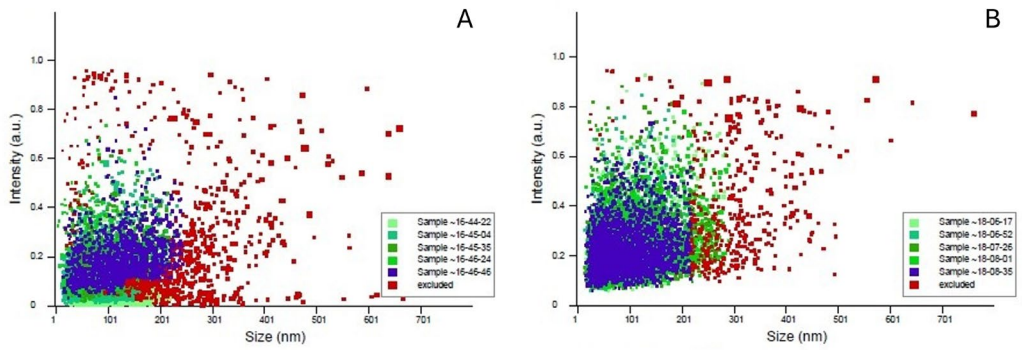

Figure 7. Nanoparticle Tracking Analysis (NTA) of extracellular particles. (A) Amastigote-derived sample. (B) Promastigote-derived sample. Both preparations exhibited high particle concentration and marked polydispersity, with two predominant peaks (~60–70 nm and ~150–160 nm). Larger particles represented ~9% in amastigotes and ~22% in promastigotes.

4. Discussion

This study provides a descriptive ultrastructural and fluorescence-based characterization of lipid-rich and vesicle-like structures in *Leishmania (L.) amazonensis* promastigotes and intracellular amastigotes. The observations presented here reinforce the growing recognition that lipid organization, membrane remodeling, and compartmental heterogeneity are central features of trypanosomatid cell biology [4–10]. In accordance with MISEV2023 recommendations, all

 doi:10.20944/preprints202602.1539.v1

interpretations remain strictly morphological and avoid any inference regarding vesicle identity, biogenesis, or function [23].

4.1. Lipid-Rich and Vesicle-like Structures in Promastigotes

Promastigotes displayed abundant vesicle-like compartments concentrated within the flagellar pocket, a region widely recognized as the primary site of endocytic and exocytic trafficking in *Leishmania* spp. [1–3,6]. The presence of electron-dense lipid bodies adjacent to the Golgi complex (Figure 4A) is consistent with previous descriptions of neutral lipid reservoirs in trypanosomatids, which have been associated with membrane turnover, metabolic adaptation, and responses to environmental stress [9–14]. Fluorescence microscopy using BODIPY® 493/503 confirmed the presence of neutral lipid pools, supporting the interpretation that promastigotes maintain structurally defined lipid storage compartments without implying functional roles [4,10,21].

Golgi-associated cisternal structures with morphology compatible with early autophagic processes (Figure 5) were also observed. Autophagy-related pathways have been implicated in organelle remodeling and membrane recycling in kinetoplastids [8,12]. Although such structures may intersect with lipid-associated remodeling events, the present study does not assign mechanistic significance to these observations.

4.2. Lipid-Rich Inclusions in Intracellular Amastigotes

Intracellular amastigotes exhibited distinct lipid-rich inclusions within parasitophorous vacuoles (Figure 4B). These findings align with reports describing stage-specific metabolic adaptations in amastigotes, including altered lipid utilization, membrane reorganization, and modulation of the vacuolar microenvironment [5,8,9,14]. SEM imaging revealed rounded amastigotes with surface protrusions (Figure 3), consistent with morphological adaptations to the intracellular niche [11,12]. Although lipid-derived molecules from *Leishmania* have been implicated in immunomodulatory processes [1–3,5,7–10,14], the present observations remain strictly structural and do not support functional conclusions.

4.3. Heterogeneity of Extracellular Particles Detected by NTA

Nanoparticle Tracking Analysis revealed stage-dependent differences in particle abundance and size distribution. Amastigote-derived supernatants contained higher particle concentrations (3.1–5.9 × 10^8 particles/mL) and smaller mean diameters (132–171 nm), whereas promastigotes exhibited broader distributions and larger modal sizes (~241 nm). These patterns are compatible with the heterogeneous particulate landscape previously described in trypanosomatids [10,17–20]. The combined filtration–ultrafiltration–ExoSpin workflow revealed two predominant peaks (~60–70 nm and ~150–160 nm) in both stages, further highlighting polydispersity. In strict accordance with MISEV2023, these particles are interpreted solely as submicron particles detected by NTA, without assumptions regarding their identity, origin, or biological relevance [23].

4.4. Methodological Considerations and Limitations

The integration of TEM, SEM, fluorescence microscopy, and NTA provided a comprehensive morphological overview of lipid-rich structures in *L. amazonensis*. However, several limitations must be acknowledged:

- no isolation or purification of extracellular vesicles was performed;no biochemical or proteomic characterization was conducted;
- no functional assays were included;
- no organelle-specific markers were applied;
- no controls for particle purity or co-isolated contaminants were incorporated.

Consequently, all structures described here should be interpreted as morphological features compatible with membrane-associated processes, rather than confirmed extracellular vesicles or

 doi:10.20944/preprints202602.1539.v1

defined organelles. This descriptive approach is intentional and consistent with the study's scope and with current EV reporting standards [23].

4.5. Implications for Future Research

The structural diversity documented in this study provides a foundation for future investigations integrating lipidomics, biochemical profiling, standardized EV isolation workflows, and functional assays. Comparative analyses across *Leishmania* species and related trypanosomatids may further clarify how lipid-rich compartments contribute to parasite adaptation, membrane remodeling, and host–parasite interactions [10,19–24]. By establishing a detailed morphological baseline, the present findings support the development of mechanistic studies aimed at elucidating the roles of lipid-associated structures in parasite physiology and pathogenesis.

The conceptual framework illustrated in Figure 8 situates the cellular and morphological observations of this study within broader evolutionary and ecological perspectives relevant to *Leishmania* biology. Although the present work focuses exclusively on descriptive ultrastructural and fluorescence-based analyses, several theoretical frameworks—including Evo-Devo [7], niche theory [8], epigenetic regulation [16], and Red Queen co-evolutionary dynamics [24]—provide useful conceptual contexts for interpreting how membrane-associated and lipid-rich structures may contribute to parasite adaptation across diverse environments.

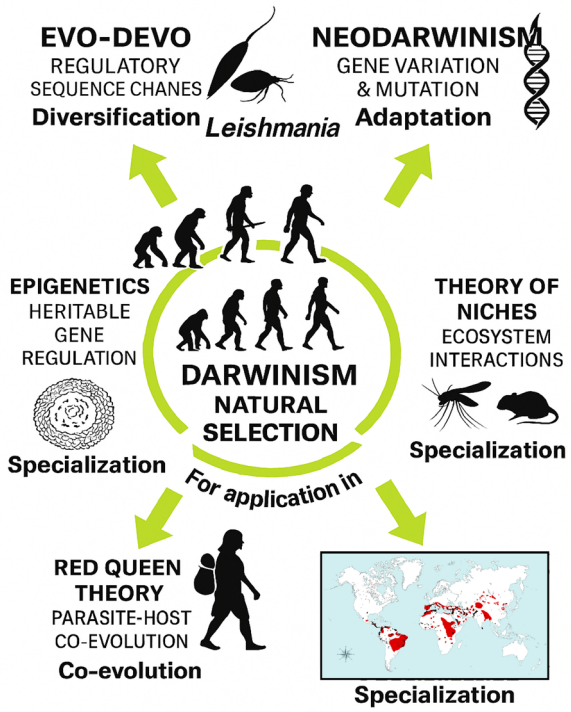

Figure 8. Conceptual diagram illustrating Darwinian foundations and evolutionary extensions relevant to Leishmania research. The central theme of natural selection is represented by hominid silhouettes, with arrows indicating five theoretical domains: (1) Evo-Devo, emphasizing developmental diversification [16]; (2) Neodarwinism, highlighting genetic variation; (3) Niche Theory, focusing on ecological interactions [17]; (4) Epigenetics, referring to heritable regulatory mechanisms [18]; and (5) Red Queen Theory, illustrating parasite–host co-evolution [19,20]. A world map depicts the global distribution of zoonotic Leishmania species. This figure provides a conceptual framework—not derived from experimental data—and complements the comparative information summarized in Supplementary Table S1.

The presence of lipid-rich and vesicle-like compartments in *L. (L.) amazonensis* is compatible with models proposing that membrane-based communication systems support parasite survival, host

 doi:10.20944/preprints202602.1539.v1

exploitation, and ecological specialization. Similar hypotheses have been raised in comparative studies involving related trypanosomatids such as *Trypanosoma cruzi* [15]. However, these interpretations remain speculative and are not directly addressed by the experimental data presented here. The figure therefore serves as a conceptual illustration rather than an empirical extension of the results, and its purpose is to contextualize the morphological findings within established evolutionary theory.

This broader evolutionary perspective is particularly relevant for zoonotic *Leishmania* species, whose ecological distribution, vector associations, and host-range diversification remain major global health challenges [1,20]. By integrating ultrastructural observations with methodological and conceptual insights, the present study supports a working model in which lipid-centered and membrane-associated processes may contribute to parasite adaptation, intracellular persistence, and long-term ecological trajectories [1–14,16–24]. Although the functional significance of these structures cannot be inferred from the current data, their consistent presence across parasite stages highlights their potential relevance for future investigations into therapeutic targets, biomarker discovery, and standardized EV-related research pipelines [19–23].

5. Conclusions

This This study provides a descriptive ultrastructural and fluorescence-based characterization of lipid-rich and vesicle-like structures in *Leishmania (L.) amazonensis*. Promastigotes displayed membrane-derived compartments concentrated in the flagellar pocket and lipid bodies adjacent to the Golgi complex, while intracellular amastigotes exhibited lipid-rich inclusions within parasitophorous vacuoles. BODIPY® staining confirmed the presence of neutral lipid pools, supporting the interpretation that both parasite stages maintain active lipid storage and membrane-associated remodeling processes. NTA revealed stage-dependent differences in particle abundance, size distribution, and polydispersity in culture supernatants. Together, these findings provide morphological context for future studies integrating ultrastructure, lipidomics, biochemical profiling, and functional assays to elucidate the roles of lipid-rich structures in parasite biology and host–parasite interactions.

Supplementary Materials: The following supporting information can be downloaded at: Preprints.org.

Author Contributions: The authors contributed equally to the work. Roles: resources, conceptualization, investigation, formal analysis, writing, review and editing, Á.M.G.; investigation, writing, review and editing, A.G.-P.; resources, investigation, formal analysis, writing, review and editing, W.L.A.P.; investigation, formal analysis, writing, review and editing, K.W.P.; resources, formal analysis, supervision, writing, review and editing E.O.d.S. All authors have read and agreed to the published version of the manuscript.

Funding: This research was supported by the Coordination for the Improvement of Higher Education Personnel (CAPES) and by the Portuguese Foundation for Science and Technology (FCT), through the research project GHTM–UID/Multi/04413/2013 and Portugal-Brazil research project PTDC/SAU-PAR/28459/2017 EXOTRYPANO IHMT-NOVA/FMV-ULisboa/UFRN.

Institutional Review Board Statement: The study was approved by the Ethics Committee on Animal Use (CEUA/UFPA) under protocol number 4847221118 (ID 001134).

Data Availability Statement: The data presented in this study are available on request from the corresponding author (Á.M.G.). The data is not publicly available due to confidentiality.

Acknowledgments: All the authors of the manuscript acknowledge their respective laboratories/institutes/universities and would like to thank the anonymous reviewers for their thoughtful comments and efforts towards improving the manuscript. Á.M.G. gratefully acknowledge the Laboratory of Gabriela Santos-Gomes IHMT-UNL-Portugal for her permanent support, scientific guidance and thesis supervision.

 doi:10.20944/preprints202602.1539.v1

Conflicts of Interest: The authors declare no conflict of interest.

Abbreviations

The following abbreviations are used in this manuscript:

BODIPY Boron-dipyrromethene
CRISPR Clustered regularly interspaced short palindromic repeats
DNA Desoxyribonucleic acid
EM Electron microscopy
EV Extracellular vesicle
FA Fatty acid
GPI Glycosylphosphatidylinositol
LD Lipid droplet
LEV Leishmania extracellular vesicle
LC-MS/MS Liquid chromatography–tandem mass spectrometry
MS Mass spectrometry
NTA — Nanoparticle Tracking Analysis
PBS Phosphate-buffered saline
RNA Ribonucleic acid
TEM Transmission electron microscopy
EvoDevo Evolutionary developmental biology
RQT Red Queen Theory

References

1. World Health Organization (WHO). *Leishmaniasis*; WHO Fact Sheet, April 2017. Available online: https://www.who.int/mediacentre/factsheets/fs375/en/ (accessed on 24 July 2017).
2. Atayde, V.D.; Hassani, K.; da Silva Lira Filho, A.; et al. Extracellular Vesicles in *Leishmania* Infection: Modulators of Host–Parasite Interaction. *PLoS Pathog.* 2023, *19*, e1012636. https://doi.org/10.1371/journal.ppat.1012636..
3. Silverman, J.M.; Clos, J.; de'Oliveira, C.C.; et al. *Leishmania* Exosomes Modulate Innate Immunity and Promote Infection. *Proc. Natl. Acad. Sci. USA* 2010, *107*, 21635–21640. https://doi.org/10.1073/pnas.1006042107..
4. Parreira de Aquino, G.; et al. Lipid Metabolism in *Leishmania*: Implications for Pathogenesis and Drug Resistance. *Microb. Cell* 2021, *8*, 88–104. https://doi.org/10.15698/mic2021.02.741..
5. Chowdhury, S.; et al. Host–Parasite Lipid Interactions in Leishmaniasis: Mechanisms and Therapeutic Perspectives. *Int. J. Mol. Sci.* 2022, *23*, 2414. https://doi.org/10.3390/ijms23112414..
6. Rodrigues, J.C.F.; et al. Metabolic Adaptations of *Leishmania* Parasites: Lipid Remodeling and Survival Strategies. *Microorganisms* 2023, *13*, 531. https://doi.org/10.3390/microorganisms13030531..
7. Carroll, S.B. Evo Devo and the Evolution of Animal Diversity. *Cell* 2005, *120*, 201–207. https://doi.org/10.1016/j.cell.2005.01.020..
8. Hutchinson, G.E. Concluding Remarks. *Cold Spring Harb. Symp. Quant. Biol.* 1957, *22*, 415–427. https://doi.org/10.1101/SQB.1957.022.01.039..
9. Kumar, A.; et al. Lipid-Mediated Modulation of Host Immunity by *Leishmania* spp. *Exp. Parasitol.* 2021, *223*, 107999. https://doi.org/10.1016/j.exppara.2021.107999..
10. Macedo, A.M.; et al. Lipidomic Signatures of *Leishmania* Extracellular Vesicles Reveal Species-Specific Patterns. *Int. J. Mol. Sci.* 2023, *24*, 10637. https://doi.org/10.3390/ijms241310637..
11. Pal, P.; Das, S.; Chatterjee, N.; Bose, D.; Saha, K.D. Studies on the Anti-Inflammatory Effect of Leishmanial Lipid In Vitro and In Vivo. *Prajnan O Sadhona* 2015, *2*, 1–XX.
12. Serrano, A.; et al. Lipid Droplets and Vesicular Trafficking in *Leishmania*: Ultrastructural Insights. *Micron* 2021, *142*, 103089. https://doi.org/10.1016/j.micron.2021.103089..

 doi:10.20944/preprints202602.1539.v1

13. Sacks, D.; et al. Lipid Bodies in *Leishmania*: Structure, Function, and Role in Host Interaction. *Mol. Biochem. Parasitol.* 2009, *165*, 1–9. https://doi.org/10.1016/j.molbiopara.2009.07.004..
14. Parreira de Aquino, G.; et al. Lipid Remodeling in *Leishmania*: A Microbial Cell Perspective. *Microb. Cell* 2021, *8*, 1–12. https://doi.org/10.15698/mic2021.01.741..
15. Booth, L.-A.; Smith, T.K. Lipid Metabolism in *Trypanosoma cruzi*: A Review. *Mol. Biochem. Parasitol.* 2020, *240*, 111324. https://doi.org/10.1016/j.molbiopara.2020.111324..
16. Bird, A. Perceptions of Epigenetics. *Nature* 2007, *447*, 396–398. https://doi.org/10.1038/nature05913..
17. Gonçalves, R.; et al. Extracellular Vesicles from Protozoan Parasites: Biogenesis, Composition, and Function. *Front. Microbiol.* 2016, *7*, 427. https://doi.org/10.3389/fmicb.2016.00427..
18. Costa, D.L.; et al. Lipid-Rich Extracellular Vesicles in *Leishmania* Infection: Implications for Pathogenesis. *Int. J. Parasitol.* 2024, *54*, 1–18. https://doi.org/10.1016/j.ijpara.2024.01.004..
19. Gabriel, Á.M.; Galué Parra, A.; Pereira, W.L.A.; Pedersen, K.W.; da Silva, E.O. *Leishmania* 360°: Guidelines for Exosomal Research. *Microorganisms* 2021, *9*, 2081. https://doi.org/10.3390/microorganisms9102081..
20. Gabriel, Á.M.; Galvão, G.R.; Galué Parra, A.; Casseb, L.M.N.; Pereira, W.L.A.; Pedersen, K.W.; Aguiar, D.C.F.; Gonçalves, E.C.; da Silva, E.O. Pathogenesis of Canine Leishmaniasis: Diagnostic Accuracy and Experimental Models Targeting *Leishmania* Lipid-Bound Vesicles. *Acad. Biol.* 2025, *3*(1), 1–XX. https://doi.org/10.20935/AcadBiol7491..
21. Santos, L.C.; et al. Metabolomic Profiling of *Leishmania* Species Reveals Lipid Remodeling During Infection. *Metabolites* 2024, *14*, 658. https://doi.org/10.3390/metabo14120658..
22. Kim, S.E.; Ibarra-Meneses, A.V.; Fernandez-Prada, C.; Huan, T. Global Lipidomics Reveals the Lipid Composition Heterogeneity of Extracellular Vesicles from Drug-Resistant *Leishmania*. *Metabolites* 2024, *14*, 658. https://doi.org/10.3390/metabo14120658..
23. International Society for Extracellular Vesicles (ISEV). MISEV2023: Minimal Information for Studies of Extracellular Vesicles. *J. Extracell. Vesicles* 2023. Available online: https://isevjournals.onlinelibrary.wiley.com/doi/10.1002/jev2.12404 (accessed on 7 January 2026).
24. Schmid-Hempel, P. *Evolutionary Parasitology*; Oxford University Press: Oxford, UK, 2011. ISBN 978-0199229482.